Imaging a full set of optical scattering properties of biological tissue by inverse spectroscopic optical coherence tomography

Ji Yi* and Vadim Backman

Department of Biomedical Engineering, Northwestern University, 2145 Sheridan Road, Evanston, Illinois 60208, USA
**Corresponding author: ji-yi@northwestern.edu*

Received June 13, 2012; revised September 20, 2012; accepted September 21, 2012;
posted September 21, 2012 (Doc. ID 170534); published October 23, 2012

We here develop a method to measure and image the full optical scattering properties by inverse spectroscopic optical coherence tomography (ISOCT). Tissue is modelled as a medium with continuous refractive index (RI) fluctuation and such a fluctuation is described by the RI correlation functions. Under the first-order Born approximation, the forward model is established for ISOCT. By measuring optical quantities of tissue including the scattering power of the OCT spectrum, the reflection albedo α defined as the ratio of scattering coefficient μ_s, and the backscattering coefficient μ_b, we are able to inversely deduce the RI correlation function and image the full set of optical scattering properties. © 2012 Optical Society of America

OCIS codes: 170.4500, 290.3200, 290.5820.

As an important approach to provide quantitative guidance for disease diagnosis or screening, measurement of tissue optical properties plays a key role in biophotonics research. Methods have been developed to measure optical properties in various ways. [1] Imaging techniques, such as confocal reflectance microscopy [2], optical coherence tomography (OCT) [3], and quantitative phase imaging [4] are able to quantify spatially resolved optical properties. However, the above-mentioned methods are insufficient to measure the full set of optical properties *in vivo* due to the backscattering detection scheme for noninvasive measurement, which only allows sampling over a small angular extent of the scattering field.

Here, we propose a novel methodology to measure and image the full set of optical properties using inverse spectroscopic optical coherence tomography (ISOCT). The forward model of ISOCT regards tissue as a medium with a continuously varying refractive index (RI). Since RI fluctuation in tissue is weak, the optical scattering properties can be derived under the first-order Born approximation. By the optical measurement of OCT, the RI spatial auto-correlation (RI correlation) function can be reversely deduced, and the entire optical scattering properties can be quantified. More importantly, the three-dimensional (3D) imaging capability of OCT provides localized analysis, which helps to directly visualize the optical properties.

The most comprehensive way to quantify a random continuous medium is to use the RI correlation function, which statistically characterizes the tissue structural distribution. We modelled the RI correlation function $C_n(\rho)$ by the Whittle–Matern (WM) functional family with three parameters: the deterministic factor D, the length scale of the correlation l_c, and the scaling factor $\mathcal{N}_c$. The WM functional family covers essentially all the well-known functions. When $0 < D < 3$, the correlation function has the form of a power law for small ρ. When $3 < D < 4$, the correlation function forms a stretched exponential. When $D = 4$, the correlation function evolves into an exponential and approaches a Gaussian function when D goes infinity. l_c determines the upper length scale of the correlation function, beyond which the function rolls off to 0 quickly. $\mathcal{N}_c$ is a scaling factor representing the variance of the RI fluctuation.

$$C_n(\rho) = \mathcal{N}_c \cdot 2^{(5-D)/2}\left(\frac{\rho}{l_c}\right)^{(D-3)/2} K_{(D-3)/2}\left(\frac{\rho}{l_c}\right), \quad (1)$$

in which $K_\nu(\cdot)$ denotes the modified Bessel function of the second kind, and ρ is the spatial displacement.

Under the Born approximation, the differential scattering cross section per unit volume σ toward any direction can be analytically derived [5]

$$\sigma(\theta,\phi) = 2\mathcal{N}_c k^4 l_c^3 \Gamma(D/2)\frac{(1-\sin^2(\theta)\cos^2(\phi))}{\sqrt{\pi}(1+[2kl_c\sin(\theta/2)]^2)^{D/2}}, \quad (2)$$

where (θ,ϕ) denotes the scattering angle in a spherical coordinate system, k is the wave number, Γ denotes the gamma function, and $(1-\sin^2(\theta)\cos^2(\phi))$ is the dipole factor with linearly polarized incidence on $\phi = 0$ direction. We next defined the backscattering coefficient $\mu_b = 4\pi\sigma_b$, where σ_b is the backscattering cross section per unit volume when $\theta = \pi$,

$$\mu_b = \mathcal{N}_c 8\sqrt{\pi}\Gamma(D/2)k^4 l_c^3 (1+[2kl_c]^2)^{-D/2}. \quad (3)$$

Meanwhile, the scattering coefficient μ_s is by definition an integration of σ over all solid angles.

$$\begin{aligned}\mu_s = \mathcal{N}_c \frac{\sqrt{\pi}\Gamma(D/2-3)}{2k^2 l_c^3}[&(1+(2k^2l_c^2(D/2-2)-1)\\ &\times 2k^2l_c^2(D/2-3)) - (1+2k^2l_c^2(D/2+1)\\ &+4k^4l_c^4(4-3D/2+D^2/4))(1+4k^2l_c^2)^{1-D/2}]. \quad (4)\end{aligned}$$

The reflection albedo α, defined here as the ratio of μ_b and μ_s, can then be written. Tissue usually satisfies $kl_c \gg 1$ [6] and $D > 2$ according to the later measurements. Under this condition, the expression of μ_b and μ_s can be simplified:

 © 2012 Optical Society of America

$$\mu_b \approx 2^{3-D}\mathcal{N}_c\sqrt{\pi}\Gamma(D/2)l_c^{3-D}k^{4-D}, \qquad (kl_c \gg 1)$$
$$\mu_s \approx 2\mathcal{N}_c\sqrt{\pi}\Gamma(D/2-1)k^2 l_c, \qquad (kl_c \gg 1 \,\&\, D > 2); \quad (5)$$

thus

$$\alpha \approx \Gamma(D/2)/\Gamma(D/2-1)(2kl_c)^{2-D}. \quad (6)$$

The phase function essentially has the shape of $\sigma(\theta,\phi)$ only with normalization such that the integral over 4π is equal to unity. The anisotropic factor g is defined as the cosine average $\langle\cos(\theta)\rangle$ of the phase function, and is also a function of D, kl_c. [5] Since it has been derived previously, we will not repeat the equation here.

With the forward model, we attempt to solve the inverse problem for ISOCT. Since OCT has small NA, the squared intensity of OCT image I^2 is approximately proportional to the backscattering coefficient μ_b [7,8]:

$$I^2 = rI_0^2\frac{\mu_b}{4\pi}L\exp(-2z n\mu_s), \quad (7)$$

where I_0 and L is the intensity and the temporal coherence length of the incidence, respectively; r is the reference reflectance coefficient, z is the depth, and n is the mean RI of the tissue, taken as 1.38. As Fig. 1 shows, the maximum value of the I^2 measures μ_b, and the decay rate along depth measures μ_s based on Beer's law. Thus the reflection albedo α can be calculated. Further, the spectrum of μ_b can be analysed by the time-Fourier analysis in spectroscopic OCT [9], and fitted with a power law equation. The exponent [often called the scattering power (SP)] is equal to $4-D$ according to Eq. (5). With D and α, l_c can be deduced according to Eq. (6). Then the correlation functional form can be readily described by D and l_c. Therefore, the phase function in Eq. (2) and g can be quantified.

Experimentally, we used a conventional Fourier-domain OCT (FDOCT) system with a supercontinuum source providing an illumination bandwidth from 650 to 800 nm. The axial resolution is ~1.5 μm, and the lateral resolution is ~10 μm with an effective NA 0.04. The scanning range is 2×2 mm on the lateral plane ($x\times y$) and the B-scan rate is 10 fps. The spectra were first normalized by the reference spectrum and the OCT A-lines were normalized by the intensity profile of the focused beam. The OCT spectra were extracted by a short frequency Fourier transform (SFFT) [9] with a spectral resolution of 15 nm, relaxing the axial resolution to ~15 μm.

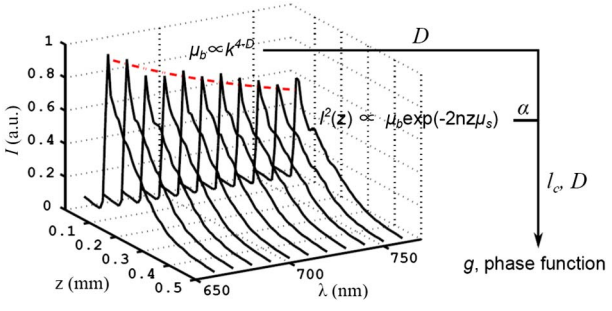

Fig. 1. (Color online) Schematic of the methodology. D is obtained from power law fitting to μ_b spectrum. l_c is deduced by D and α according to Eq. (6).

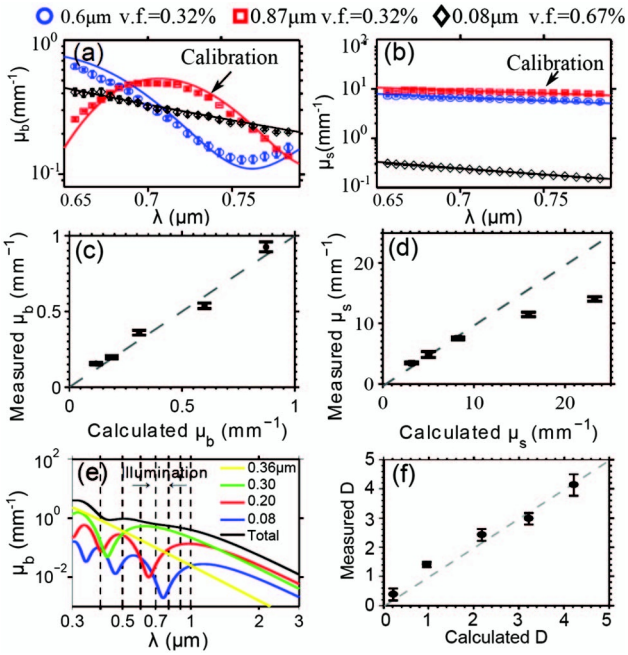

Fig. 2. (a) and (b) μ_b and μ_s spectrum with the sphere diameters and volume fraction (v.f.). (c) and (d) Calibration of μ_b and μ_s in various concentrations of 0.87 μm spheres. (e) D value phantom design with four types of spheres. The total spectrum is a power law within the illumination bandwidth. (f) Calibration of D. All the measurements were repeated three times. Error bar = S.E.

To characterize our measurement, we first fabricated a solid Agarose gel phantom embedded with polystyrene microspheres. The averaged signal was obtained from 0.5×0.5 mm^2 lateral area (in $x\times y$). The measurements of μ_b and μ_s were repeated at each wavelength during SFFT according to Eq. (7). As Figs. 2(a) and 2(b) show, the experiment agrees with Mie theory (solid line) well and the error is within 0.05 and 0.22 mm^{-1} for μ_b and μ_s, respectively. Due to the finite spectral resolution in SFFT, the Mie spectra were smoothed with 15 nm Gaussian windows. Further, we used 0.87 μm spheres phantom, varied the concentration and compared the averaged μ_b and μ_s over λ to the Mie prediction as in Figs. 2(c) and 2(d). μ_b fits with the calculated value well over a range up to 1 mm^{-1} and μ_s deviates from around 14 mm^{-1}, above which multiple scattering starts contributing the signal.

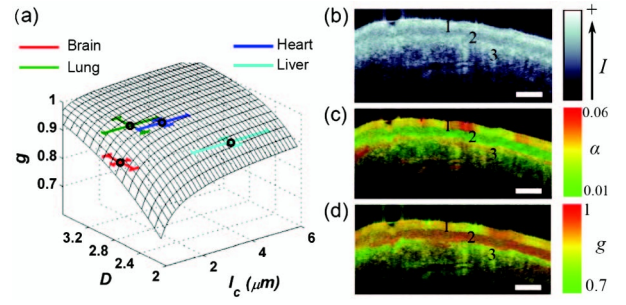

Fig. 3. (a) Map of g dependence on D and l_c. (b)–(d) Conventional OCT, α and g image from a rat buccal sample. (1) Keratinized epithelium, (2) stratified squamous epithelium, and (3) submucosa. Bar = 50 μm.

Table 1. Physical and Optical Properties ±S.E. of Different Rat Organs (710 nm)

	N	D	μ_s (mm^{-1})	μ_b (mm^{-1})	l_c (μm)[a]	g[a]	g from literature [1]
Brain	6	2.80 ± 0.21	10.81 ± 0.28	0.65 ± 0.08	0.76 ± 0.29	0.87 ± 0.05	0.88 (633 nm)
Liver	10	2.36 ± 0.11	10.32 ± 0.29	0.49 ± 0.03	4.05 ± 1.52	0.91 ± 0.02	0.95 (630 nm)
Lung (deflated)	9	3.02 ± 0.20	11.42 ± 0.29	0.11 ± 0.02	1.75 ± 1.04	0.95 ± 0.04	0.95 (630 nm)
Heart	9	2.84 ± 0.08	13.26 ± 0.37	0.27 ± 0.06	2.59 ± 0.96	0.96 ± 0.02	0.973–0.983 (1060 nm)
Intestine	7	3.06 ± 0.15	7.80 ± 0.23	0.05 ± 0.01	2.78 ± 1.42	0.97 ± 0.03	
Spleen	7	2.98 ± 0.19	13.28 ± 0.30	0.26 ± 0.09	1.71 ± 1.13	0.95 ± 0.03	

[a]Data were deduced and averaged from each measurement.

Next we characterized the accuracy of measuring D from the SP. A phantom with different polystyrene microsphere composition was designed as Fig. 2(e) shows. The total spectrum smooths out the individual oscillatory spectra from each size of microsphere and exhibits a power law over the incident bandwidth. The averaged spectra were obtained over 0.05×1 mm^2 area in $x \times y$. Figure 2(f) plots the comparison of D on our measurements with the calculated values, which is calculated from Mie theory according to Eq. (5). We used four sizes of spheres (diameter: 360, 300, 200, and 80 nm) to compose the phantoms, and the volume ratio of spheres for individual D values are 0/6/5/0 ($D = 4.12$), 6/20/60/0 ($D = 3.42$), 6/20/60/150 ($D = 2.26$), 6/15/60/1000 ($D = 0.98$), and 0/0/0/1 ($D = 0.12$). The accuracy of D measurement is ±0.20 with 90% confidence using a linear regression on the calibration curve. Combining the calibration of μ_b and μ_s, the accuracy of measuring g is within ±0.03.

With the system calibrated, we measured six rat organs *ex vivo* to demonstrate the feasibility of ISOCT. μ_s and μ_b were calculated from the entire bandwidth, so that l_c is calculated at the center wavelength 710 nm in Eq. (6). With D and l_c, g were obtained as shown in Fig. 3(a) for four types of organs. The key parameters of the tested organs from one subject are summarized in Table 1. To justify our measurement, the g values of similar organs from the literature are listed as comparison. Each measurement is taken over 0.25×0.25 mm^2 area in $x \times y$ and from the top 100 μm tissue.

Figures 3(c) and 3(d) further demonstrate the capacity of imaging optical properties from an *ex vivo* rat buccal sample. The α and g values designate hue, and the image intensity encodes saturation and value in the hue, saturation, value (HSV) space. Three prominent layers are keratinized epithelium (KE), stratified squamous epithelium (SE), and submucosa (SM), each of which is considered homogeneous and applicable to our method. The SE appears more translucent and its anisotropic factor is measured at 0.91 on average, compared the KE and SM at 0.85 and 0.81 on average, respectively. For a robust measurement, μ_s and μ_b were smoothed over lateral 0.05×0.25 mm^2 area in $x \times y$ for each layer and D is averaged over the entire layer. The attenuation along the depth is compensated by multiplying the A-line signal with an exponential function according to μ_s [10].

The key assumption of the model is the first-order Born approximation. Although discontinuity at boundaries exists in tissue, the small RI changes can still satisfy the approximation and thus the derivation from RI correlation function to the optical properties is still applicable [6].

The authors acknowledge the financial support from National Institutes of Health (NIH) grants R01CA128641 and R01EB003682 and National Science Foundation (NSF) grant CBET-0937987.

References

1. W. Cheong, S. Prahl, and A. Welch, IEEE J. Quantum Electron. **26**, 2166 (1990).
2. T. Collier, M. Follen, A. Malpica, and R. Richards-Kortum, Appl. Opt. **44**, 2072 (2005).
3. D. Faber, F. van der Meer, M. Aalders, and T. van Leeuwen, Opt. Express **12**, 4353 (2004).
4. H. Ding, Z. Wang, X. Liang, S. A. Boppart, K. Tangella, and G. Popescu, Opt. Lett. **36**, 2281 (2011).
5. J. D. Rogers, İ. R. Çapoğlu, and V. Backman, Opt. Lett. **34**, 1891 (2009).
6. İ. R. Çapoğlu, J. D. Rogers, A. Taflove, and V. Backman, Opt. Lett. **34**, 2679 (2009).
7. V. M. Kodach, D. J. Faber, J. van Marle, T. G. van Leeuwen, and J. Kalkman, Opt. Express **19**, 6131 (2011).
8. N. Bosschaart, D. J. Faber, T. G. van Leeuwen, and M. C. G. Aalders, J. Biomed. Opt. **16**, 030503 (2011).
9. R. Leitgeb, M. Wojtkowski, A. Kowalczyk, C. K. Hitzenberger, M. Sticker, and A. F. Fercher, Opt. Lett. **25**, 820 (2000).
10. C. Xu, J. M. Schmitt, S. G. Carlier, and R. Virmani, J. Biomed. Opt. **13**, 034003 (2008).